Progress in Additive Manufacturing (2024) 9:947–957
https://doi.org/10.1007/s40964-023-00494-9

FULL RESEARCH ARTICLE

Influence of heat treatment on the mechanical performance of Ti21S octet truss lattice structure fabricated by laser powder bed fusion

A. Jam[1,6] · M. Pellizzari[1] · L. Emanuelli[2] · G. Valsecchi[3] · A. du Plessis[4,5] · M. Benedetti[1]

Received: 2 May 2023 / Accepted: 5 August 2023 / Published online: 18 August 2023

Abstract

Additive manufacturing allows the production of complex and custom designs including lattice structures—porous metallic structures with designed porosity and tailored mechanical properties. The bulk material has a key influence on the eventual properties of the porous lattice structure material. Among metallic biomaterials, beta-titanium alloys are gaining increasing interested because of their low Young's modulus. In this work, the heat treatment of beta-Ti21S alloy is investigated in the context of octet truss lattice structures. The intention is to improve the performance of these structures for their reliable use in biomedical applications such as for bone implants. The study makes use of laser powder bed fusion of representative samples, uses microCT for physical characterization of manufacturing quality, while quasi-static and fatigue testing is performed to evaluate the performance of these lattice structures. The results indicate that the heat treatment significantly improves the fatigue properties of the lattice structures while changing the quasi-static failure mode more towards a stretch-based failure mode. These findings have practical implications for the implementation of this material and structure combination in medical implants. By enhancing the performance of the lattice structures, the study paves the way for their reliable use in biomedical applications.

Keywords Beta-Ti21S alloy · Laser powder bed fusion · Heat treatment · Octet truss lattices · Fatigue strength

1 Introduction

The study of metallic lattice materials has gained popularity in recent decades due to advancements in form-freedom fabrication techniques [1]. These techniques have improved the ability to control the size and shape of lattice materials, making them highly useful in biomedical applications [2].

The most commonly used method for fabrication of biomedical components is metal additive manufacturing, specifically the powder bed fusion process [3]. In this process, thermal energy from an electron or laser source is used to melt a powder bed and create the desired shape. Laser-based powder bed fusion of metals (PBF-LB/M) provides better surface roughness and more precise geometry than electron-based powder bed fusion (PBF-EB/M) [4]. As a result, PBF-LB/M is better suited for fabricating complex and intricate biomedical components with fine features and high quality.

Despite its ability to fabricate feature sizes as small as 0.1 mm in complex geometries, the properties of final geometries produced using PBF-LB/M are still a concern for load-bearing applications. This issue has been studied in the context of defect tolerant lattice structures made of beta-Ti 21S alloy [5]. In Ref. [5], it was found that micro-notches present in the rough surface, or highly localized stress raiser locations, on the surface of the lattice were the primary cause of premature failure and reduced mechanical properties. The negative impact of these micro-notches was greater when the cell size was less than 4 mm, or when the strut thickness was below 0.64 mm. Therefore, it is crucial to assess the

✉ M. Benedetti
matteo.benedetti@unitn.it

1 Department of Industrial Engineering, University of Trento, Trento, Italy

2 INSTM (Operative Center, University of Trento), Via Sommarive 9, Trento, Italy

3 TAV Vacuum Furnaces Inc., Caravaggio, BG, Italy

4 Research Group 3D Innovation, Stellenbosch University, Stellenbosch, South Africa

5 Object Research Systems, Montreal, Canada

6 Present Address: National Center for Additive Manufacturing Excellence (NCAME), Mechanical Engineering Department, Auburn University, Auburn, USA

manufacturability of simple geometries in various cell sizes before attempting to fabricate complicated geometries.

Present beta-Ti21S alloy exhibits remarkable mechanical properties already in the as-built state with a low elastic modulus required for biomedical application [6]. Nevertheless, the rapid heating and solidification rate during PBF-LB promote the structural and microstructural anisotropy inside the material, formation of microsegregation and presence of residual stress deleterious for the mechanical and stability response of the part. A lot of studies consider the effect of different heat treatments on the most common Ti alloy used in the biomedical field, namely Ti–6Al–4V [7–11]. Seyed Alireza Etsami et al. demonstrated that the Ti–6Al–4V heat treated below β transus temperature (T_β) is characterized by increased ductility due to the formation of $\alpha+\beta$ lamellar structure [7]. Zhiyi Zou et al., proposed new heat treatments based on the refinement of the prior-β grains thanks to rapid heat treatments in the β phase field leading to increased strength without loss in ductility [10]. A dual stage heat treatment was proposed by Jinlong Su et al. to obtain a strengthened bimodal microstructure [11]. The effect of heat treatment on Ti–6Al–7Nb, a non-cytotoxic vanadium-free alloy, in comparison with Ti–6Al–4V was investigated by Chao Xu et al. The authors demonstrated that a solution treatment above the β transus permits to meet the biomedical standards [12]. In the last years, metastable β-Ti alloys produced by additive manufacturing gained increasing interest respect to the conventionally forged alloys. Proper post-heat treatments were studied to improve both, microstructure and properties [13–17]. In case of metastable β Ti alloys, a solubilization at a temperature below T_β ensured optimal combination of fine β grain and sufficient β dissolution. The aging treatment at temperature between 500 and 700 °C after solubilization led to the precipitation of α phase with a morphology depending on the aging temperature. The mechanical properties could be tuned accordingly [13]. Considering the metastable β Ti21S, excellent results in terms of strength–ductility ratio were achieved by heat treating the wrought alloy [18, 19]. To the authors best knowledge, just a few papers report about the influence of heat treatment on microstructure and properties of Ti21S produced by PBF [20], none of them dealing with lattice structures. Investigations are needed to exploit the use of the heat-treated alloy for cellular structures, e.g., for lightweight design or biomedical applications.

The current work focuses on the octet truss topology, whose cell size of 4 mm was selected based on manufacturability assessments done in Ref. [5]. The octet truss topology has some advantages over other topologies in the biomedical field: (i) it has two types of different pore sizes enabling better osseointegration, leading to better biocompatibility. The small pore size contributes toward better initial cell seeding by providing surface availability for cell attachment in which low permeability is required while the big pore size enables nutrients to flow easily through the structure in which good permeability is required [21]; (ii) the octet truss topology itself provides the isotropic material properties because it has symmetric design. It has been reported that material properties of lattices depend on the loading direction [22], assuming the same fabrication quality achieved. Moreover, the octet truss is less sensitive to the building direction if the comparison is made to the other topological design [1], mainly because the building direction in AM should be strictly selected in the way that the downward faces are avoided.

The octet truss topology belongs to the strut-based architecture category, which is the most widely used category in various applications. The deformation behavior of strut-based lattices can be described based on the Maxwell stability criterion [23]. This discriminates the lattice behavior according to the sign of the coefficient $M=b-3j+6$, where b is the number of struts and j is the number of nodes. Under compression loading, strut-based lattices can collapse in two ways: (i) through rotation of the struts about the joint if $M<0$ (bending-dominated mechanism), or (ii) through axial tensile and compression loading of the struts if $M\geq 0$ (stretching-dominated mechanism). The octet truss topology theoretically follows the stretching-dominated mechanism where $M=0$, resulting in higher weight efficiency and modulus compared to bending-dominated materials [24, 25]. However, these models do not consider the influence of constitutive material properties, such as microstructural properties (i.e., internal defects, grain morphology, and phases) and intrinsic mechanical properties (elastic modulus, yield stress, and ductility), on the deformation behavior of lattices.

The influence of microstructure on the mechanical behavior of additively manufactured lattices has been limitedly studied [26, 27]. Babamiri et al. [26] investigated the relationship between the manufacturing variables, such as post-processing heat treatment, and the quasi-static and dynamic behavior of various lattice topologies made of ductile Inconel 718 material, including the octet truss topology. The heat treatment affected the microstructure of the lattice material, wherein the improved grain morphology led to an increase in flow stress by 25% in a 4 mm unit cell size with a 0.689 mm strut diameter. Another study by Duport et al. [27] explored the impact of microstructure optimization on the mechanical behavior of a binary beta-Ti-14Mo octet truss lattice fabricated by PBF-EB. The mechanical behavior of three different microstructures ($\alpha+\beta$; metastable β; and $\beta+\omega_{iso}$) were compared. The as-built $\alpha+\beta$ microstructure showed unstable post-yielding behavior under compression loading, while the heat-treated microstructure ($\beta+\omega_{iso}$) had increased tolerance to plastic buckling and stabilized post-yielding behavior, making it suitable for energy absorption applications. The precipitation of ω phase is detrimental to

ductility of Ti21S, so that this alloy is typically aged in the alpha phase temperature field to obtain a precipitation-hardened β microstructure, whose strength is mostly controlled by the volume fraction and morphology of α precipitates. A fine intragranular precipitation of α has been recommended to achieve the best strength to density ratio [28, 29]. These studies highlight the significance of material properties on the mechanics of lattices. However, further research is needed to fully understand the impact on all materials and lattice configurations.

The X-ray microcomputed tomography scan (microCT) is one of the main tools used to study lattice materials [30]. It has become an established and effective method in the additive manufacturing (AM) lattice field for not only dimensional measurement, but also for investigating failure mechanisms, due to its accuracy and ability to capture and highlight crucial sites in 3D. This makes the microCT technique superior to traditional 2D characterization methods like microscopic investigation. As a result, this method has gained popularity in recent years for investigating AM lattice structures. For example, Kolken et al. [31] used the microCT method to study the morphological properties and fatigue failure mechanism of an auxetic Ti–6Al–4V lattice, while also using digital image correlation (DIC) in 2D to study the fatigue failure mechanism. While the DIC method provides online data, it has a limitation in data analysis at high fatigue frequencies. The microCT method, on the other hand, provides 3D observations of samples without the need for a flat 2D section.

This study aims to evaluate the potential of Ti21S octet truss lattices for biomedical applications. To this end, the octet truss topology has been optimized for better manufacturability and reduced elastic modulus. Cubic lattices were manufactured using a PBF-LB process, and their morphological properties were studied using microCT. The impact of heat treatment, in particular of direct aging at 590 °C, on the mechanical properties of the constitutive material was also analyzed. Finally, the static and fatigue mechanical properties of the lattices were evaluated, and the failure mechanisms were explored using CT data from failed fatigue-tested samples.

2 Experimental materials and methods

The experimentation was carried out on specimens additively manufactured via laser powder bed fusion (L-PBF) using a pre-alloyed β-Ti21S powder produced by plasma atomization (GKN Hoeganaes Corporation, Cinnaminson, NJ, USA). For this purpose, an L-PBF machine model MYS-INT100 (SISMA, Piovene Rocchete, VI, Italy) with a laser spot of 55 µm was employed. The machine is equipped with a building platform of 100 mm diameter and a 200 W fiber laser. An XY alternate scan strategy was adopted along with a powder layer thickness of 20 µm. Some of the specimens were subjected to a post-processing heat treatment. This was carried out in TAV furnace and prior to all heating stages, chamber was subjected to vacuum 5×10^{-4} mbar followed by argon backfilling to prevent oxidation. The heat treatment strategy aimed at avoiding the precipitation of undesired brittle ω phase (see [20] for further information) and was performed according to the ASTM B265 standard [32]: the samples were heat treated at 590 °C with a heating rate of 10 °C/min, a dwell time of 8 h, and a cooling rate of 30 °C/min.

To characterize the quasi-static tensile properties, cylindrical bars were printed along the longitudinal axis. From these bars, dog-bone specimens (with 5 mm gage diameter) were machined and tested using a servo-hydraulic universal testing machine INSTRON 8516 (Instron, Nordwood, MA, USA), equipped with hydraulic grips, a load cell of 100 kN (non-linearity $\pm 0.1\%$ of R.O.) and an axial extensometer (12.5 mm gage length, non-linearity $\pm 0.15\%$ of R. O.). The yield strength was determined as the 0.2% offset yield stress.

The focus of the experimentation was on cubic lattice specimens. A careful reader may object that the impact of post-heat treatment could have been explored on conventional bulk tensile specimens as well. However, it should be noted that lattice specimens have distinct stress conditions, with localized stress peaks at the nodes that are absent in bulk coupons. During high-cycle fatigue tests, the stress state of bulk coupons remains in the elastic regime. As a result, the effect of strain softening on the fatigue strength, which is expected in lattice components, cannot be observed in the latter case.

The lattice coupons were made up of a $6 \times 6 \times 6$ arrangement of octet truss unit cells as depicted in Fig. 1. The unit cell size was set to 4 mm, based on the manufacturing feasibility established in Ref. [5]. Using the NTopology software (NTop, New York, NY, USA), the nodes of each unit cell were filleted to reduce stress concentration in these critical fatigue locations. Porosity, strut size, and fillet radius were optimized to achieve a homogenized Young's modulus of approximately 3.5 GPa, making these structures potentially suitable for use in prosthetic implants. The optimal values are listed in Table 1. It is worth mentioning that the strut thickness of 0.63 mm is very close to the value found in Ref. [5] and has been shown to provide good manufacturability and excellent static mechanical properties.

A total of 24 lattice coupons were fabricated, with half of them undergoing heat treatment. The lattice specimens underwent both quasi-static and cyclic mechanical testing. The quasi-static tests were performed using the aforementioned servo-hydraulic testing machine with compression plates, in accordance with standard ISO 13314:2011 [33]. The tests were conducted at room temperature with a constant actuator speed of 0.5 mm/min, and a linear variable

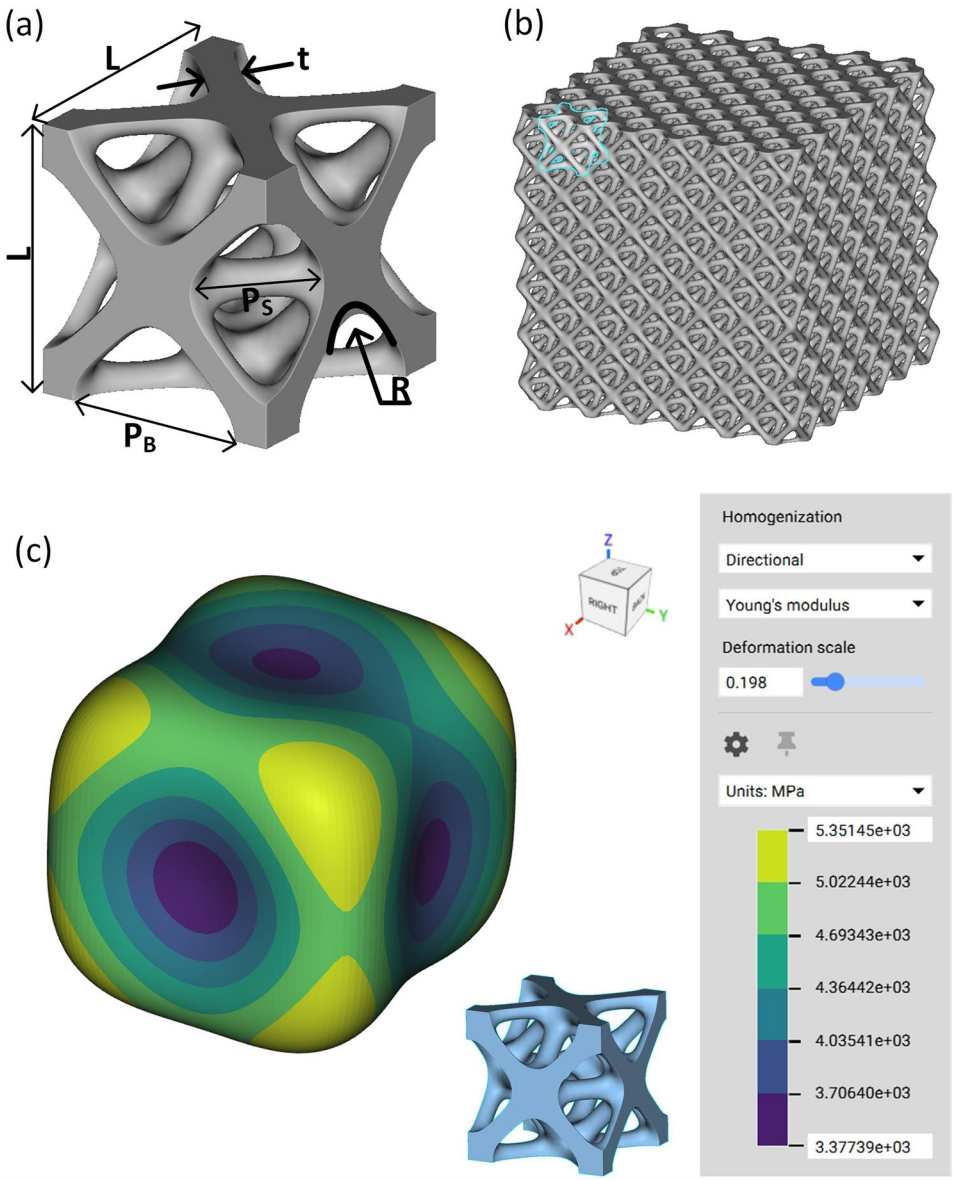

Fig. 1 **a** Definition of unit cell parameters of octet truss architecture (R = fillet radius, t = strut thickness, L = cell size or strut length, $P_{B\ and\ S}$ = big and small porosities), **b** 3D view of the repeated unit cell, **c** homogenization simulation result-directional elastic modulus for the unit cell

Table 1 Dimensions of the investigated lattices design and main processing parameters

Topology	Unit cell size	Strut thickness	Fillet radius	Relative density	porosity	Laser heat input	Scan strategy
	L (mm)	t (mm)	R (mm)	(%)	(%)	(J/mm^3)	
Optimized octet truss	4	0.63	0.6	26	73	60–90	Hatching and outer contour

displacement transducer (LVDT) was used to measure the displacement up to 15% elongation. The resulting stress–strain curve was used to calculate the monotonic Young's modulus (E_m), 0.2% offset yield strength (σ_y), and maximum compressive strength (σ_{mc}). The cyclic tests were done to obtain the cyclic Young's modulus (E_c) after the stress–strain response stabilized. The specimens were loaded between 20 and 70% of the yield load obtained from the monotonic testing using a triangular wave shape for five cycles. High-cycle compression–compression fatigue testing was performed using a Rumul Testronic (Russenberger Prüfmaschinen, Neuhausen am Rheinfall, Switzerland) resonant fatigue test machine equipped with a 50 kN load cell with a load ratio R of 0.1 in compression. Fatigue tests were run in laboratory environment at various stress amplitudes to evaluate fatigue lives ranging from

1×10^5 to 1×10^7 cycles. Each *S–N* curve was determined using around 12 specimens; run-out tests were stopped at 1×10^7 cycles when no fracture occurred. Specimens were regarded as failed if they underwent a drop in stiffness larger than 10%.

Each *S–N* curve included at least one run-out test and was interpolated using an asymptotic equation to accurately depict the knee shape of the experimental *S–N* data:

$$\sigma_{\max} = C_1 + \frac{C_2}{N_f^m}, \tag{1}$$

where $\sigma_{\max}$ is the maximum homogenized stress and N_f the number of cycles to failure. The scatter of the experimental data was determined by assessing the estimated regression variance, considered to be non-varying in the whole investigated fatigue range, and defined as

$$S^2 = \frac{\sum_{i=1}^{n} \left(\sigma_{\max,i} - \hat{\sigma}_{\max,i}\right)^2}{n - p}; \tag{2}$$

where $\sigma_{\max,i}$ are the i-th fatigue data point, $\hat{\sigma}_{\max,i}$ are their estimators, n is the number of experimental data points and p is the number of parameters in the regression (3 in the present case).

MicroCT scans were performed using a Nanotom S system (General Electric, Niskayuna, NY, USA), and analysis performed in Dragonfly software (Object Research Systems, Inc, Montreal, Quebec, Canada). Local wall thickness was evaluated using the mesh thickness function, and cracks were identified in cross-sectional images and 3D rendering used to visualize these locations.

3 Results and discussion

3.1 Microstructure and bulk mechanical properties

The microstructure of the alloy as-built reveals evidence of rapid solidification during L-PBF. Specifically, the melt pool boundaries and an extremely fine cellular structure are visible (see Fig. 2a). The high cooling rate facilitated the formation of a fully beta-metastable structure without any secondary precipitates. A detailed account of the microstructure of the as-built alloy is presented in Ref. [6]. The solidification microstructure is still discernible in the heat-treated sample (Fig. 2b), with evidence of the original columnar grains and melting pools. Although most α precipitates are intragranular, some small α grain boundary colonies are visible upon closer inspection, as indicated by SEM micrographs. The alpha lamellae, which are smaller than 1 µm, grow from the grain boundary towards the center of the grain (α_{WBG}). Alternatively, they can nucleate inside the grain, forming a knitted/beam arrangement (α_{WM}), with certain preferred orientations that are related to the growth direction and the parent β-structure. Despite the visibility of the melting pool boundaries, they do not appear to have an impact on the precipitation of α.

The monotonic tensile properties of the β-Ti21S alloy in both as-built and heat-treated conditions are compared in Table 2 with the minimum values prescribed by ASTM F2924-14 for the golden standard biomedical Ti-grade 23 (Ti–6Al–4V ELI). In Fig. 3, the monotonic stress–strain curves are plotted. It can be noted that the β-Ti21S alloy is compliant with the ASTM F2924-14 [34] prescription only in the heat-treated state. In addition, this post-process

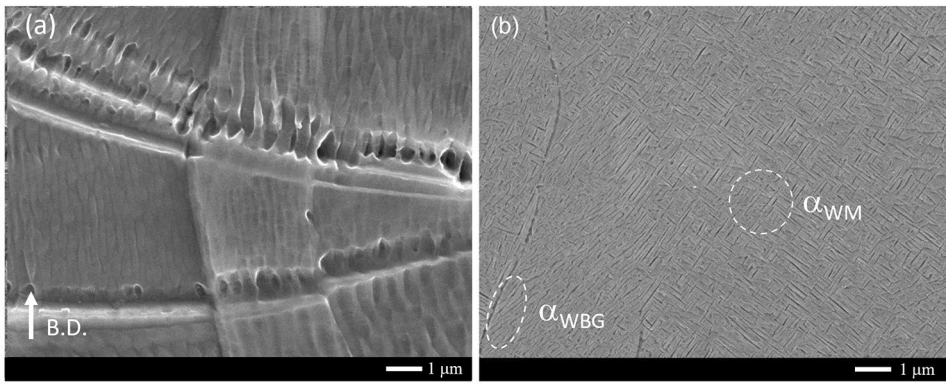

Fig. 2 SEM micrographs of **a** As-built, and **b** heat treated (590 °C/8 h) β-Ti21S alloy tensile test sample. (B.D: indicates the building direction, α_{WBG} is the Widmanstätten Grain Boundary alpha phase, and α_{WM} is the intragranular Widmanstätten alpha phase with knitted/beam arrangement

Table 2 Comparable mechanical properties of β-Ti21S and Ti–6Al–4V tensile solid samples fabricated by L-PBF

Alloy	Condition	$\sigma_{0.2}$ (MPa)	UTS (MPa)	E (GPa)	EI (%)	Structure	References
Ti21S	As-built	709 ± 6	831 ± 3	52 ± 0.3	21.6 ± 1.0	β	[6]
Ti21S	Heat treated	1208 ± 19	1235 ± 15	95.8 ± 1.1	21.0 ± 1.2	α + β	This work
Ti–6Al–4V	Heat treated	990 ± 5	1095 ± 10	110 ± 5.0	8.1 ± 0.3	α′	[29]

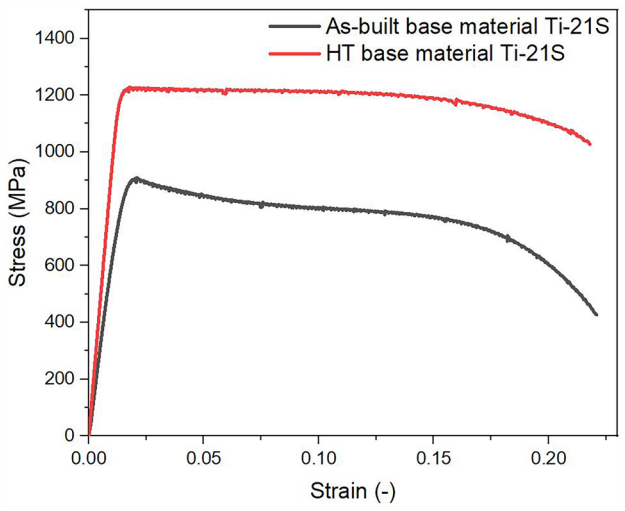

Fig. 3 Quasi-static tensile engineering stress–engineering strain curves of the β-Ti21S alloy in as-built and heat-treated condition

treatment permits to eliminate the strain softening displayed by the as-built condition and typical of many metastable β-Ti alloys [35, 36].

3.2 Metrological analyses of lattices

MicroCT analysis of the local wall thickness reveals, as expected, some increased thickness in the joints, indicating > 1 mm in these regions while the struts have a thickness of 0.5 mm. This can be seen in Fig. 4a, b, while (c) shows a cross-sectional image of the actual sample compared to the design. This latter comparison shows good build quality with some excess material in the down-skin regions only. Detailed information extracted from these 3D analyses are included in Table 3. The comparison of the same 3D information from design file allows simple evaluation, showing that the lattice is manufactured very close to the expected parameters.

3.3 Mechanical properties of lattices

Representative monotonic stress–strain curves are compared in Fig. 5 and Table 4. It can be observed that despite being nominally categorized as stretch-dominated, the specimen in its as-built condition exhibits a gradual transition to a long flat stress plateau. This can be attributed to the strain softening localized at the nodes which behave as plastic hinges making the global response of the structure bending-dominated after yielding. The high strain energy absorbed before final failure indicates the potential use of lattices in as-built conditions for energy absorbing applications. Suppressing the strain softening through heat treatment leads to a pure stretch-dominated behavior. This is characterized by

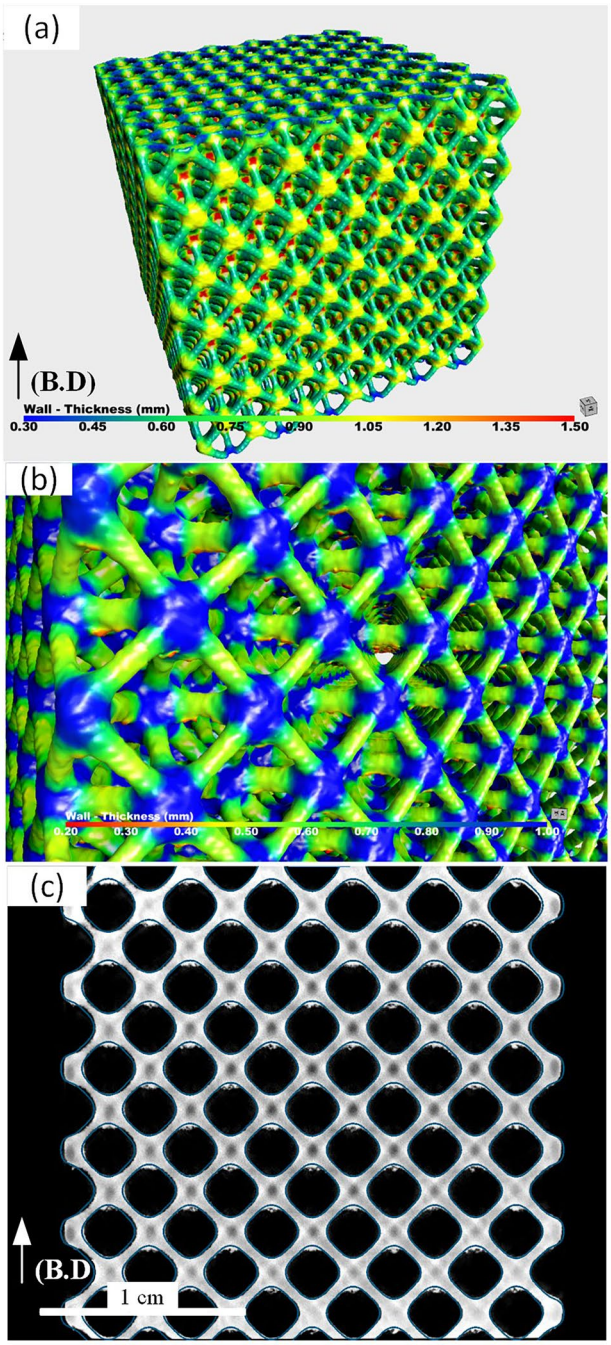

Fig. 4 **a**, **b** Wall thickness analysis for the reconstructed microCT data of optimized octet truss lattice structure, **c** the cross-section plane from the reconstructed microCT data showing the CAD deviation based on the X-ray absorption

a sudden, post-yielding collapse at stress levels much higher than the plateau observed in the as-built condition at the cost of a very limited strain to failure.

The results of compression–compression high-cycle fatigue tests are plotted in Fig. 6a, b in terms of homogenized maximum axial stress σ_{max} and normalized stress

Table 3 The morphological properties of optimized octet truss lattice structure

Relative density (%)		Strut size (mm)		Node size (mm)		Pore size (mm)	
As-designed	Dry weighing	CAD	MicroCT	CAD	MicroCT	CAD	MicroCT
26	25	0.633 ± 0.003	0.548 ± 0.002	1.034 ± 0.002	1.094 ± 0.002	Small = 1.49 ± 0.00 Big = 2.31 ± 0.00	1.23 ± 0.02 2.11 ± 0.00

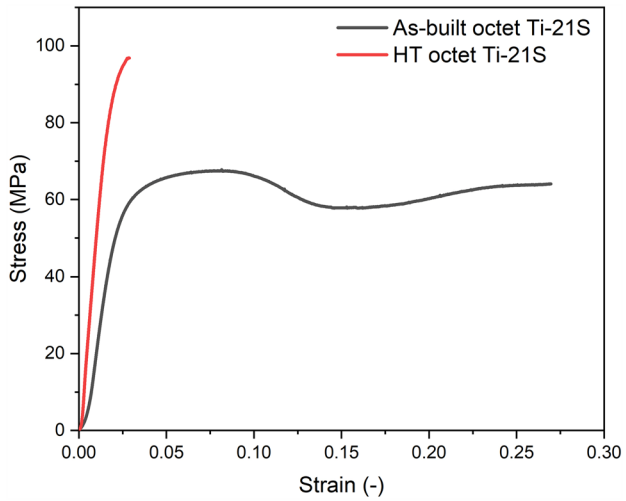

Fig. 5 Monotonic stress–strain curves of as-built and heat-treated optimized octet truss lattice structures of β-Ti21S alloy

Table 4 The morphological mechanical properties of As-built and heat-treated optimized octet truss lattice structures of β-Ti21S alloy, reported according to the ISO13314

	As-built	Heat-treated
Yield stress (MPa)	50.91 ± 0.88	76.01 ± 0.94
Quasi-elastic gradient (MPa)	3555	5408

to the compressive yield strength σ_y, respectively. Best-fit coefficients C_1, C_2, m of Eq. 1 and standard deviation S are provided in the legend of Fig. 6. It can be noted that the heat treatment considerably improves the fatigue strength, not only in terms of absolute but also relative axial stress. In particular, the HCF strength at 1×10^7 cycles is increased by almost 120%. Suppressing strain softening appears to be effective in improving the fatigue strength of lattice structures. This can be attributed to the fact that the high stress concentration in the nodes of lattice specimens leads to localized plasticization, which expands with each cycle during the fatigue tests of as-built specimens due to the strain softening. As depicted in Fig. 7, this unfavorable outcome not only reduces the fatigue strength, but also results in a noticeable and premature reduction in the stiffness of the as-built samples during fatigue tests. These results indicate

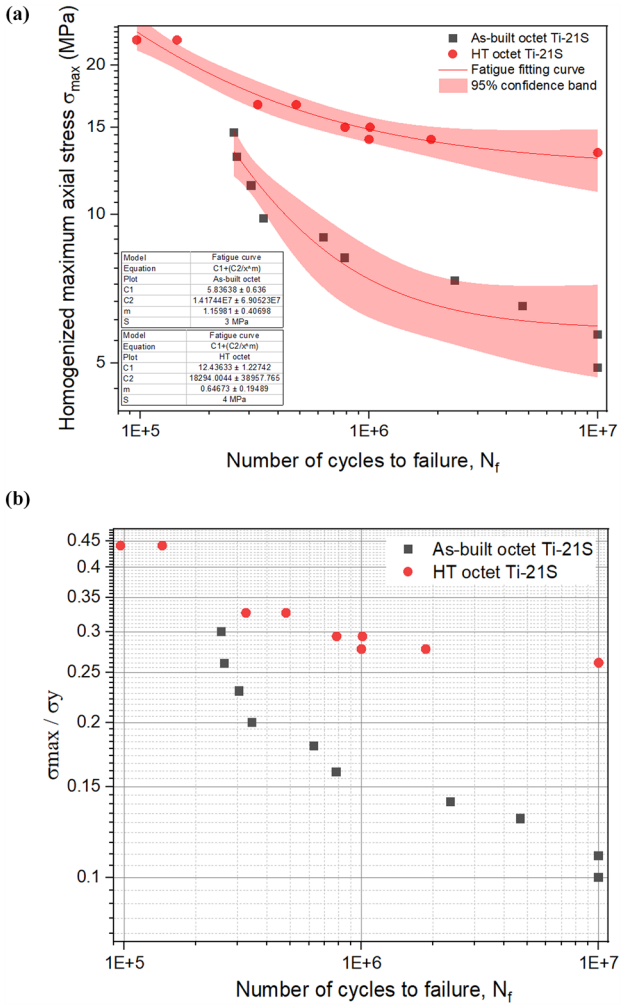

Fig. 6 SN curves of as-built and heat-treated optimized octet truss lattice structures made of β-Ti21S alloy (**a**), and same graph with maximum axial stress σ_{max} normalized with respect to the yield strength σ_y (**b**)

that lattice specimens under variable loads should undergo heat treatment prior to use. The heat treatment enhances the normalized high-cycle fatigue strength to above 0.25, which can be considered a remarkable achievement compared to the fatigue strength data published in the literature [1].

The CT scans and SEM inspections of fatigued samples are depicted in Figs. 8 and 9, respectively. It can be observed that the as-built specimens exhibit diffused fatigue damage in the form of cracks that have formed at multiple locations

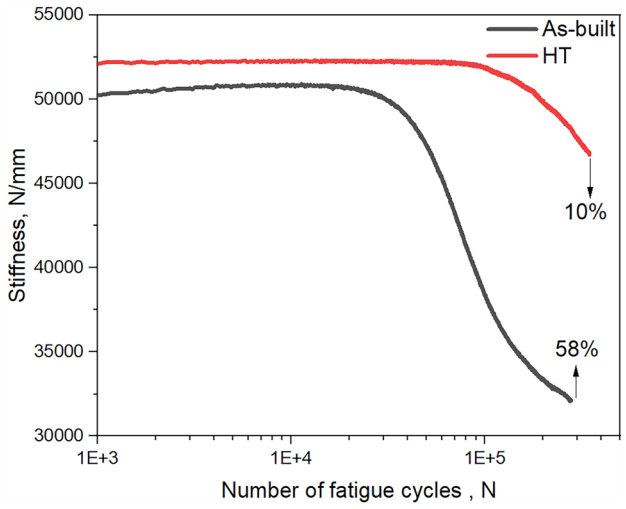

Fig. 7 Stiffness vs. number of fatigue cycles for as-built and heat-treated (HT) octet truss samples recorded during fatigue tests performed at a maximum homogenized stress of 15.6 MPa. The remarkable loss in stiffness in the as-built conditions is ascribed to the strain softening exhibited by the base material in this microstructural condition

in both the struts and nodes (Figs. 8a, 9a). This behavior is similar to that seen in cubic lattices tested in Ref. [5]. Surface imperfections, acting as stress concentrators, serve as preferential crack initiation sites (Fig. 9c). In contrast, fatigue failure in heat-treated lattices is confined to the fillet roots at the nodes only (Figs. 8b, 9b). The suppression of the strain softening mechanism seems to have eliminated the impact of the micro-notches on the strut surface (Fig. 9d).

4 Conclusions

The mechanical performance of Ti21S alloy octet truss lattice structure fabricated by laser powder bed fusion has been evaluated in the as-built state as well as after direct ageing at 590 °C for 8 h. The following main results were obtained:

- The as-built bulk alloy is characterized by a beta-metastable cellular microstructure showing good mechanical strength-ductility combination, and a marked strain softening. The heat treatment causes a fine precipitation of intragranular α and promotes a remarkable increase in

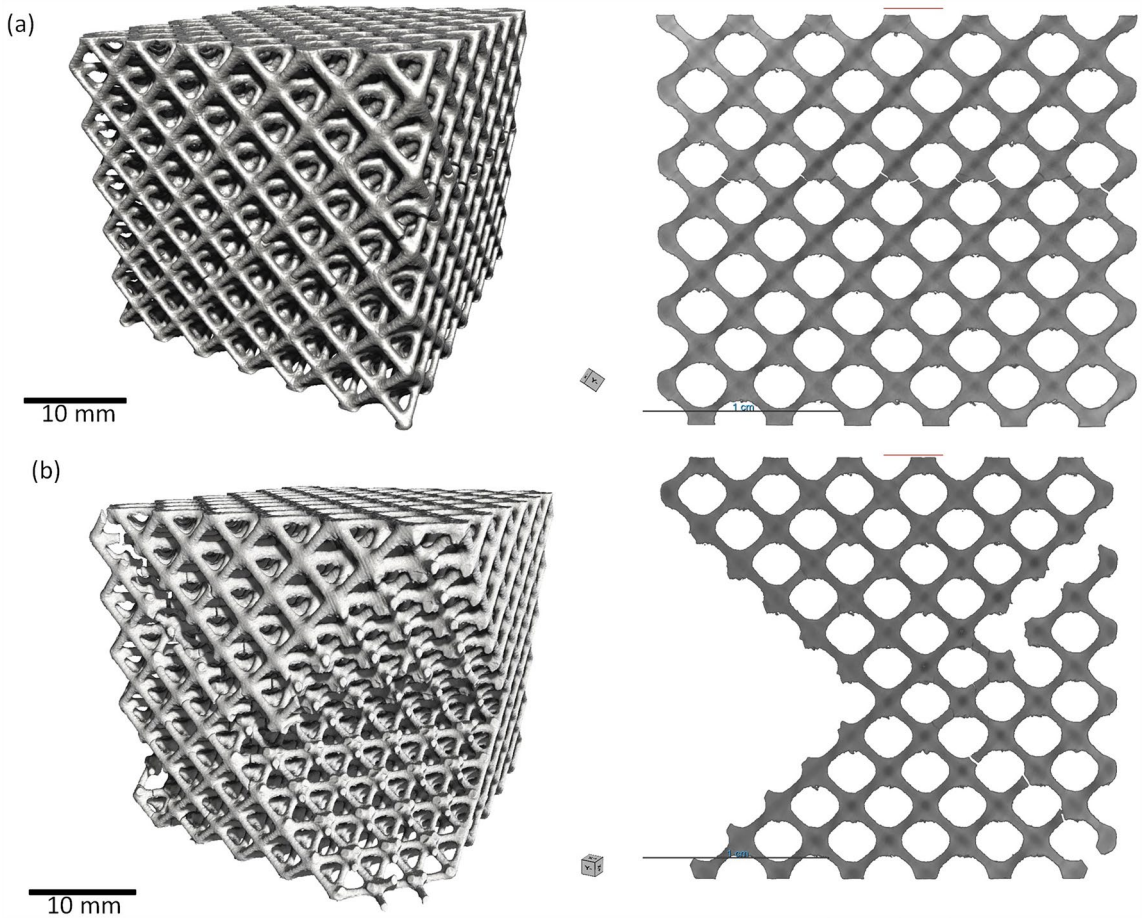

Fig. 8 **a** As-built and **b** heat-treated fatigue samples showing the failure mechanism and locations. Left: isometric, right: front view

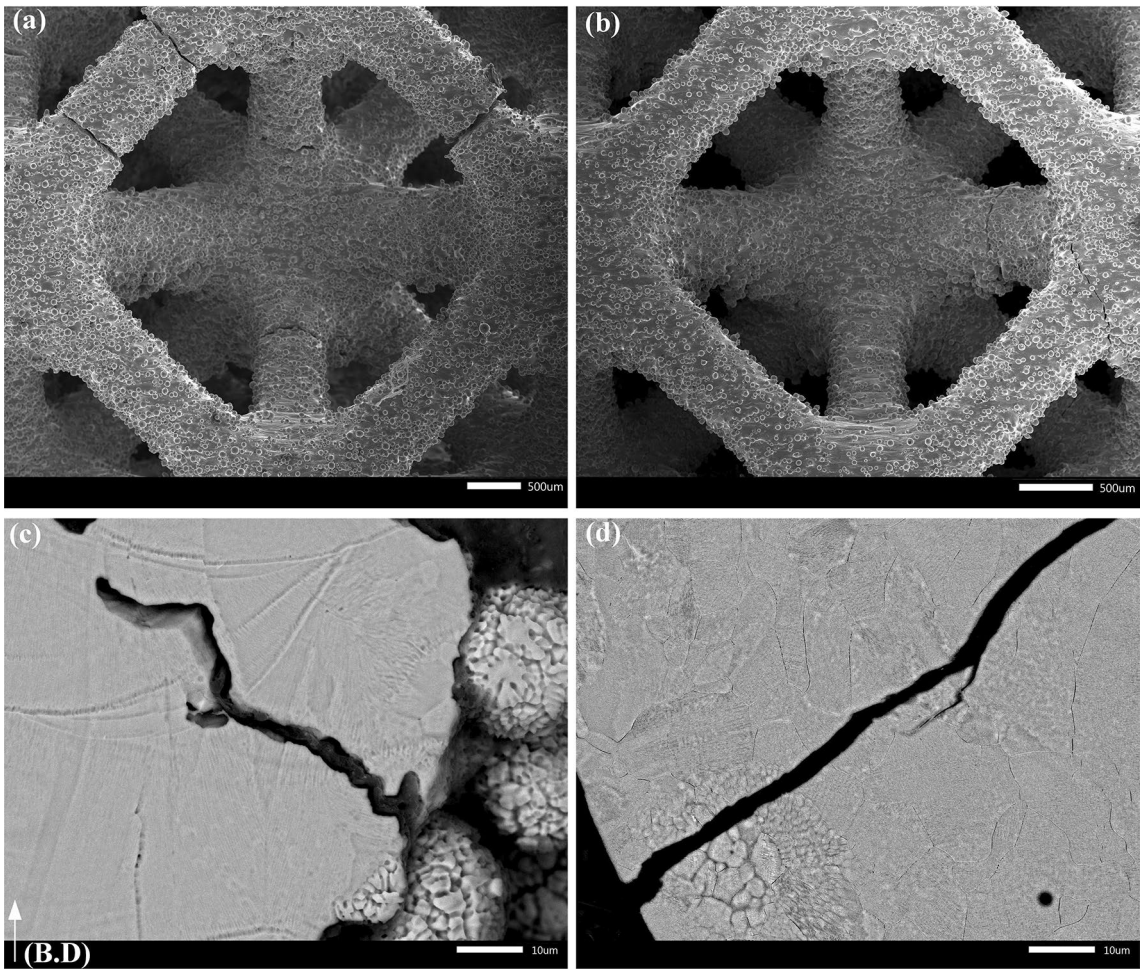

Fig. 9 SEM micrographs of **a**–**c** As-built and **b**–**d** heat-treated fatigued samples showing the failure mechanism. It is preferentially located at nodes in heat-treated samples **d** and distributed throughout the struts in as-built specimens (**c**)

strength and elastic modulus with no change in fracture elongation, and further eliminates strain softening.

- MicroCT scans were used for detailed characterization of the structure indicating good build quality lacking defects. Post-fatigue samples were used to visualize the crack locations in 3D showing all cracks occur on struts and near nodes but not through nodes.
- The monotonic stress compression tests on the lattice structures evidence that suppressing the strain softening through heat treatment leads from the pure bending-dominated behavior of as-built sample to a pure stretch-dominated behavior.
- The heat treatment considerably improves the compression–compression fatigue strength of lattice structure (by almost 120%), confirming that suppressing strain softening is more effective in improving the fatigue strength of lattice structures compared to bulk specimens. This could be ascribed to the reduced localized plasticization in the nodes of lattice specimens. The diffused fatigue damage observed in as-built lattice in the form of multiple cracks in both the struts and nodes is limited to the nodes fillet roots in heat-treated lattices.

Future work will focus on evaluating the influence of heat treatment on the fatigue strength of various cell topologies (i.e., bending-dominated and triply periodic minimal surface), investigating their behavior also under high-temperature conditions.

Acknowledgements This work is part of the Fondazione Cassa di Risparmio di Verona Vicenza Belluno e Ancona project N. 2020.0042-ID 50430, "Produzione additiva di protesi ortopediche a struttura trabecolare in Ti-beta" funded by Fondazione Cariverona.

Author contributions All the authors contributed to the study conception and design. Material preparation, data collection and analysis were performed by AJ, LE and AdP. The first draft of the manuscript was written by MB and all the authors commented on previous versions of the manuscript. All the authors read and approved the final manuscript.

Funding Open access funding provided by Università degli Studi di Trento within the CRUI-CARE Agreement.

Data availability Data available on request.

Declarations

Conflict of interest The authors have no relevant financial or non-financial interests to disclose.

References

1. Benedetti M, du Plessis A, Ritchie RO, Dallago M, Razavi SMJ, Berto F (2021) Architected cellular materials: a review on their mechanical properties towards fatigue-tolerant design and fabrication. Mater Sci Eng R Rep 144:100606. https://doi.org/10.1016/j.mser.2021.100606
2. du Plessis A, Razavi SMJ, Benedetti M, Murchio S, Leary M, Watson M, Bhate D, Berto F (2022) Properties and applications of additively manufactured metallic cellular materials: a review. Prog Mater Sci 125:100918. https://doi.org/10.1016/j.pmatsci.2021.100918
3. Zadpoor AA (2019) Mechanical performance of additively manufactured meta-biomaterials. Acta Biomater 85:41–59. https://doi.org/10.1016/j.actbio.2018.12.038
4. Debroy T, Wei HL, Zuback JS, Mukherjee T, Elmer JW, Milewski JO, Beese AM, Wilson-Heid A, De A, Zhang W (2018) Additive manufacturing of metallic components—process, structure and properties. Prog Mater Sci 92:112–224. https://doi.org/10.1016/j.pmatsci.2017.10.001
5. Jam A, du Plessis A, Lora C, Raghavendra S, Pellizzari M, Benedetti M (2022) Manufacturability of lattice structures fabricated by laser powder bed fusion: a novel biomedical application of the beta Ti-21S alloy. Addit Manuf 50:102556. https://doi.org/10.1016/j.addma.2021.102556
6. Pellizzari M, Jam A, Tschon M, Fini M, Lora C, Benedetti M (2020) A 3D-printed ultra-low Young's modulus β-Ti alloy for biomedical applications. Materials 13:2792. https://doi.org/10.3390/MA13122792
7. Etesami SA, Fotovvati B, Asadi E (2022) Heat treatment of Ti-6Al-4V alloy manufactured by laser-based powder-bed fusion: Process, microstructures, and mechanical properties correlations. J Alloys Compd 895:162618. https://doi.org/10.1016/j.jallcom.2021.162618
8. Ter Haar GM, Becker TH (2018) Selective laser melting produced Ti-6Al-4V: post-process heat treatments to achieve superior tensile properties. Materials (Basel). https://doi.org/10.3390/ma11010146
9. Zou Z, Simonelli M, Katrib J, Dimitrakis G, Hague R (2021) Microstructure and tensile properties of additive manufactured Ti-6Al-4V with refined prior-β grain structure obtained by rapid heat treatment. Mater Sci Eng A 814:141271. https://doi.org/10.1016/j.msea.2021.141271
10. Zhang Y, Feng L, Zhang T, Xu H, Li J (2021) Heat treatment of additively manufactured Ti-6Al-4V alloy: microstructure and electrochemical properties. J Alloys Compd 888:161602. https://doi.org/10.1016/j.jallcom.2021.161602
11. Su J, Jiang F, Li J, Tan C, Xu Z, Xie H, Liu J, Tang J, Fu D, Zhang H, Teng J (2022) Phase transformation mechanisms, microstructural characteristics and mechanical performances of an additively manufactured Ti-6Al-4V alloy under dual-stage heat treatment. Mater Des 223:111240. https://doi.org/10.1016/j.matdes.2022.111240
12 Xu C, Sikan F, Atabay SE, Muñiz-Lerma JA, Sanchez-Mata O, Wang X, Brochu M (2020) Microstructure and mechanical behavior of as-built and heat-treated Ti-6Al-7Nb produced by laser powder bed fusion. Mater Sci Eng A. https://doi.org/10.1016/j.msea.2020.139978
13. Ramachandiran N, Asgari H, Dibia F, Eybel R, Muhammad W, Gerlich A, Toyserkani E (2023) Effects of post heat treatment on microstructure and mechanical properties of Ti5553 parts made by laser powder bed fusion. J Alloys Compd 938:168616. https://doi.org/10.1016/j.jallcom.2022.168616
14. Ackers MA, Messé OMDM, Manninen N, Stryzhyboroda O, Hecht U (2022) Additive manufacturing of TTFNZ (Ti-4.5Ta-4Fe-7.5Nb-6Zr), a novel metastable β-titanium alloy for advanced engineering applications. J Alloys Compd 920:165899. https://doi.org/10.1016/j.jallcom.2022.165899
15. Liu Y, Xu L, Qiu C (2022) Development of an additively manufactured metastable beta titanium alloy with a fully equiaxed grain structure and ultrahigh yield strength. Addit Manuf 60:103208. https://doi.org/10.1016/j.addma.2022.103208
16. Pang X, Xiong Z, Yao C, Sun J, Misra RDK, Li Z (2022) Strength and ductility optimization of laser additive manufactured metastable β titanium alloy by tuning α phase by post heat treatment. Mater Sci Eng A 831:142265. https://doi.org/10.1016/j.msea.2021.142265
17 Rajan Soundararajan S, Vishnu J, Manivasagam G, Rao Muktinutalapati N (2021) Heat treatment of metastable beta titanium alloys. Weld Mod Top. https://doi.org/10.5772/INTECHOPEN.92301
18. Boyer RR, Welsch G, Collings EW (1994) Materials properties handbook: titanium alloys. ASM International. ISBN: 978-0-87170-481-8
19. Williams JC, Boyer RR (2020) Opportunities and issues in the application of titanium alloys for aerospace components. Metals (Basel). https://doi.org/10.3390/met10060705
20. Pellizzari M, Jam A, Tonon V, Benedetti M, Lora C (2021) Ageing behavior of Beta-Ti21S produced by laser powder bed fusion. Metall Ital 113:42–49
21. Bobyn JD, Pilliar RM, Cameron HU, Weatherly GC (1980) The optimum pore size for the fixation of porous surfaced metal implants by the ingrowth of bone. Clin Orthop Relat Res. https://doi.org/10.1097/00003086-198007000-00045
22. Dallago M, Raghavendra S, Luchin V, Zappini G, Pasini D, Benedetti M (2021) The role of node fillet, unit-cell size and strut orientation on the fatigue strength of Ti-6Al-4V lattice materials additively manufactured via laser powder bed fusion. Int J Fatigue 142:105946. https://doi.org/10.1016/j.ijfatigue.2020.105946
23. Deshpande VS, Ashby MF, Fleck NA (2001) Foam topology: bending versus stretching dominated architectures. Acta Mater 49:1035–1040. https://doi.org/10.1016/S1359-6454(00)00379-7
24 Fleck NA, Deshpande VS, Ashby MF (2010) Micro-architectured materials: past, present and future. Proc R Soc A Math Phys Eng Sci 466:2495–2516. https://doi.org/10.1098/rspa.2010.0215

25 Ashby M (2006) The properties of foams and lattices. Philos Trans R Soc A Math Phys Eng Sci 364:15–30. https://doi.org/10.1098/rsta.2005.1678
26. Babamiri BB, Barnes B, Soltani-Tehrani A, Shamsaei N, Hazeli K (2021) Designing additively manufactured lattice structures based on deformation mechanisms. Addit Manuf. https://doi.org/10.1016/j.addma.2021.102143
27. Duport M, Martin G, Lhuissier P, Blandin J-J, Prima F, Dendievel R (2022) Stabilizing post-yielding behavior of a stretching dominated lattice structure through microstructural optimization. Scr Mater 219:114887. https://doi.org/10.1016/j.scriptamat.2022.114887
28 Mantri SA, Choudhuri D, Behera A, Cotton JD, Kumar N, Banerjee R (2015) Influence of fine-scale alpha precipitation on the mechanical properties of the beta titanium alloy beta-21S. Metall Mater Trans A Phys Metall Mater Sci. https://doi.org/10.1007/s11661-015-2944-y
29. Facchini L, Magalini E, Robotti P, Molinari A, Höges S, Wissenbach K (2010) Ductility of a Ti-6Al-4V alloy produced by selective laser melting of prealloyed powders. Rapid Prototyp J 16:450–459. https://doi.org/10.1108/13552541011083371
30. du Plessis A, Yadroitsev I, Yadroitsava I, le Roux SG (2018) X-Ray microcomputed tomography in additive manufacturing: a review of the current technology and applications, 3D print. Addit Manuf 5:227–247. https://doi.org/10.1089/3dp.2018.0060
31. Kolken HMA, Garcia AF, Du Plessis A, Meynen A, Rans C, Scheys L, Mirzaali MJ, Zadpoor AA (2022) Mechanisms of fatigue crack initiation and propagation in auxetic meta-biomaterials. Acta Biomater. https://doi.org/10.1016/j.actbio.2021.11.002
32. A.B.- 20a (2020) Standard specification for titanium and titanium alloy strip, sheet, and plate. https://doi.org/10.1520/B0265-20A
33. ISO 13314 (2011) ISO 13314 Mechanical testing of metals, ductility testing, compression test for porous and cellular metals, Ref. Number ISO. 13314, pp 1–7. www.iso.org
34. American Society for Testing Materials, ASTM F2924-14 (2014) Standard specification for additive manufacturing titanium-6 aluminum-4 vanadium ELI with powder bed fusion, West Conshohocken, PA, USA
35. Ramachandiran N, Asgari H, Dibia F, Eybel R, Keshavarzkermani A, Gerlich A, Toyserkani E (2023) Anisotropic tensile behavior of laser powder-bed fusion made Ti5553 parts. Mater Sci Eng A 865:144633. https://doi.org/10.1016/j.msea.2023.144633
36. Kumar SSS, Pavithra B, Singh V, Ghosal P, Raghu T (2019) Tensile anisotropy associated microstructural and microtextural evolution in a metastable beta titanium alloy. Mater Sci Eng A. https://doi.org/10.1016/j.msea.2019.01.053